

Continental-scale prediction of live fuel moisture content using soil moisture information



Vinod Vinodkumar^{a,b,*}, Imtiaz Dharssi^a, Marta Yebra^{b,c}, Paul Fox-Hughes^d

^a Bureau of Meteorology, Docklands, Melbourne, VIC, 3008, Australia

^b Bushfire and Natural Hazard Cooperative Research Centre, East Melbourne, VIC, 3002, Australia

^c Australian National University, Canberra, Australia

^d Bureau of Meteorology, Hobart, TAS, 7000, Australia

ARTICLE INFO

Keywords:

Soil moisture
Live fuel moisture
Fire
JULES
AFMS
JASMIN

ABSTRACT

Live fuel moisture content (LFMC) is a key factor that determines the flammability of vegetation in ecosystems. Soil moisture (SM) is one of the variables that is known to influence plant water use. The present study analyses the LFMC-SM relationship over Australia using gridded, remote sensing-based LFMC and land surface model-based SM products. A lag-correlation analysis conducted over 60 selected sites shows that the strength of the relationship between LFMC and SM varies from site to site and, in general, is moderately strong (median lag-correlation of ~0.5). However, the strength of the relationship changes with vegetation type and also with soil profile depth. At all the sites, SM is found to be a leading indicator of LFMC. The lag also varies with the location and is found to range from days to months. Based on the location-based correlation analysis, we identify the 0–35 cm SM profile (SM_{0-35cm}) to be the best predictor of LFMC. We developed a simple model to predict daily LFMC, where it is hypothesised that daily variations in LFMC from its annual cycle can be predicted using daily deviations from the annual cycle in SM_{0-35cm} . The annual cycles of LFMC and SM_{0-35cm} are modelled using Fourier cosine series. The averaged (over 60 sites) correlation obtained for the validation period is 0.74 when a time-lag of 14 days is assumed at all locations. When the model is applied nationally at a 5 km grid, the normalised root mean squared error for the validation period is found to be less than 25% in general. The results from the present study highlight a modelling strategy that can be used to address a critical gap in the forecast of spatially and temporally continuous LFMC at regional scales in advance for operational fire management applications.

1. Introduction

Fuel moisture content (FMC) is a critical variable affecting fire interactions with fuel and partly controls the efficiency of fire ignition and burning. The moisture content of dead fuel (forest leaf litter, twigs etc.) is found to be dependent on the atmospheric variability (Viney, 1991). It can be modelled reasonably well using weather variables (Matthews, 2013). However, the moisture content of live vegetation is more complicated because it depends on eco-physiological properties that may significantly vary among different plant species (Pellizaro et al., 2007). The living vegetation may act as a heat source or a heat sink, conditional to the moisture content and the fire heat flux, and thereby either contributing to or inhibiting fire propagation and intensity

(Nelson, 2001).

Live fuel moisture content (LFMC) is defined as a ratio of the mass of water contained within live vegetation to that of dry mass, expressed as a percentage (Yebra et al., 2019). Objectively identifying "live" fuels itself is a challenge due to the multiple stages of growth that can be found in plants at a given point of time (Kidnie et al., 2015). In general, "live" fuel denotes both green and senescing vegetations (Kidnie et al., 2015, Sharma et al., 2020). LFMC variations are related to both environmental conditions (e.g.: meteorological variables, soil water availability) and eco-physiological characteristics of the plant species (Castro et al., 2003). Research has shown that LFMC can be derived with reasonable accuracy on a continental scale using measurements from optical remote sensing-based satellite platforms (Yebra et al., 2018).

* Corresponding author at: Research Program, Science and Innovation Group, Bureau of Meteorology, 700 Collins Street, Docklands, Melbourne, Victoria, 3008, Australia.

E-mail address: vinod.kumar@bom.gov.au (V. Vinodkumar).

Such a continental scale LFMC product not only offers the large-scale observability but also provides a much higher temporal resolution and spatial coverage compared to the point-based, weekly to monthly resolution on a few locations typical of the traditional, manual observing methods. Recently, a new LFMC near-real-time product has been developed for Australia using a radiative transfer model inversion technique on MODerate-resolution Imaging Spectroradiometer (MODIS) reflectance data (Yebra et al., 2018). This LFMC product (named hereafter as AFMS-LFMC) forms the basis of the Australian Flammability Monitoring System (AFMS), a web-based interface monitoring the LFMC and soil moisture (SM) routinely across the landscapes (<http://anuwald.science/afms>). The AFMS-LFMC includes both green and senescent vegetation and follows the definition of Kidnie et al (2015).

Predicting the moisture status of live fuels is an important gap in modelling fire risk over periods of weeks to seasons. Current operational methods in Australia rely on the persistence of observed values or subjective expert assessment of the response of fuels to the forecasted rainfall anomalies. Optical remote-sensing based LFMC products lack the predictive capability desirable for fire management. Also, the sampling density is limited by the satellite over-pass frequency and cloud-cover. Therefore, it is desirable to have models that could reasonably predict the LFMC from more easily accessible parameters. The SM state is a key factor in assessing the dryness of vegetation due to the relationship that exists between the two variables (Sharma et al 2020; Nolan et al., 2020). Large wildfires are found to occur exclusively under conditions of low soil moisture (Kluger et al., 2015). Hence, traditionally, simple soil moisture (deficit) indices are used as a surrogate or to estimate parameters related to fuel dryness (Cruz et al., 2015). The Keetch-Byram Drought Index (KBDI; Keetch and Byram (1958)) and the Soil Dryness Index (SDI; Mount (1972)) are two such SM indices used in Australia. The KBDI, which measures cumulative soil water deficit in forested ecosystems, is found to exhibit a strong relationship with LFMC (Dimitrakopoulos and Bemmerzouk, 2003). There are a variety of indices in use across the world which estimate SM as a proxy for land dryness and can be related to LFMC. For example, Viegas et al. (2001) and Castro et al. (2003) found that a non-linear relationship can be derived between moisture codes in the Canadian Forest Fire Weather Index (FWI) system and LFMC data for Mediterranean vegetation.

Although estimating SM deficit indices using meteorological data is relatively easy to achieve, there are a few issues in using them to model LFMC. First, SM deficit/dryness indices are traditionally computed at weather station locations and may not be representative of larger areas. Secondly, these indices are rather simplified, empirical, water balance models that do not consider most factors that influence SM dynamics. For example, the KBDI and Soil Dryness Index (SDI) methods used operationally in Australia neglect spatial variations in soil type, vegetation type, terrain, and aspect. The above indices also over-simplify evapotranspiration and runoff processes, potentially leading to large errors in the estimated SM state. Krueger et al. (2017) found that observed soil moisture was a better predictor than KBDI over Southern Great Plains in the US for growing-season wildfires. Studies have also shown that SM from land surface models is more accurate than the above indices (Vinodkumar et al., 2017). Hence, efforts were made to develop a prototype system based on Joint UK Land Environment Simulator (JULES) land surface model (LSM) to estimate SM deficit for fire danger rating (Dharssi and Vinodkumar, 2017). This system, called the JULES based Australian Soil Moisture INformation (JASMIN; Dharssi and Vinodkumar, 2017), estimates SM at a spatial resolution of 5 km for the whole of Australia. Verification against ground-based SM observations shows that a prototype version of this system is significantly better than the KBDI and SDI models (Dharssi and Vinodkumar, 2017). The JASMIN SM is also displayed via the AFMS web interface to aid the monitoring of land dryness routinely.

The main aim of the present research is to suggest a modelling strategy to forecast LFMC on a continental scale using readily available JASMIN SM estimates. The present study can be a step forward to

provide fire agencies with a capability to estimate LFMC in advance with good accuracy. In that respect, the study, as the first aim, determines the strength of the relationship between LFMC and SM over the Australian landscape at representative locations. Moving ahead, the study develops a simple model to predict LFMC using SM as the only input data. The modelling technique discussed here is simple and can offer a constructive basis for advancing the strategy further for improving the LFMC predictions. More importantly, the study addresses the lack of a continental scale, forecasting, LFMC product which is a critical gap in the current fire management practices in Australia. One of the considerations for the data analysis presented in this study and which is relevant to the main objective here is to understand each product in the context of fire danger. Such an analysis can also be useful for practitioners in fire management agencies to understand the merit of each product. In that respect, a quantitative evaluation of AFMS-LFMC, JASMIN SM and predicted LFMC is presented for days and locations of fire occurrences identified using MODIS fire radiative power (FRP) data.

2. Datasets

2.1. Soil moisture content

The SM content data used in the present study is provided by the JASMIN system in volumetric units ($\text{m}^3 \text{ m}^{-3}$). JASMIN is based on the JULES (Best et al., 2011) land surface model. The JULES is developed by the United Kingdom Met Office in partnership with various academic and research institutions. The JASMIN system covers whole Australia at a spatial resolution of 5 km. The system runs with an hourly time step and the output is stored at every third time-step. A four-layer soil profile of total 3 m depth is defined for each grid box, where the soil is vertically homogeneous. The soil layers (depth) from surface to bottom are 0–0.1 m (0.1 m), 0.1–0.35 m (0.25 m), 0.35–1 m (0.65 m), and 1–3 m (2 m) respectively. The change in total SM content within each soil layer of JASMIN/JULES from the previous time step is based on the evapotranspiration extracted directly from the layer by plant roots, the diffusive water flux flowing in from the layer above, and the diffusive flux flowing out to the layer below (Cox et al., 1999). The SM tendency is based on a finite difference approximation of Richards's equation and Darcy's law. JASMIN uses the van Genuchten soil hydraulic model (van Genuchten, 1980) to define the relationship between SM and soil hydraulic conductivity. Transpiration by plants extracts soil water directly from the soil layers via the plant roots while bare soil evaporation extracts soil water from the topmost soil layer only. The ability of plants to access water from each soil layer is determined by the root density distribution and SM availability. The SM availability is a function of SM and soil texture. Evapotranspiration is modelled using a modified Penman/Monteith equation coupled to a photosynthesis/surface conductance model. JULES use ancillary information on land cover types, vegetation heights, soil texture, soil albedo, soil hydraulic and thermal properties, and leaf area index. The LAI ancillary information is seasonally varying whereas vegetation properties like height, land cover etc. are static. A canopy height dataset derived from space-borne light detection and ranging (LIDAR) instrument (Simard et al., 2011) is used in JASMIN for an accurate representation of tree heights in Australia.

The physical processes in LSMs are driven by meteorological data, and the frequencies by which the state variables are updated correspond to the temporal resolution of provided meteorological fields. The air temperature, specific humidity, wind speed and surface pressure data required by JASMIN is obtained from BoM's Mesoscale Surface Analysis System (MSAS; Glowacki et al., 2012). MSAS perform hourly analyses of atmospheric pressure at mean sea level, potential temperature, 2 m dew point temperature, and 10 m wind components on a ~4 km grid. This data is converted and re-gridded to drive JASMIN. The MSAS data is available from 2007 onwards and is on-going with near-real-time (~6-hour latency) updates. The downward surface shortwave radiation required by JULES is provided by an hourly product developed in

the Bureau of Meteorology based on measurements from the Himawari geostationary meteorological satellites. This product is available at a spatial resolution of 5 km. The downward surface longwave radiation data is obtained from the Bureau of Meteorology's operational regional numerical weather prediction (NWP) model (Puri et al., 2013). The NWP data is available in real-time, 6-hourly, at a resolution of 12 km. The precipitation data used to drive JASMIN is obtained from BoM's Australian Water Availability Project (AWAP; Jones et al., 2009) product. AWAP is an in-situ observations-based product and provides daily analyses of rainfall at a spatial resolution of 0.05°. The Tropical Rainfall Measuring Mission (TRMM; Huffman et al. 2007) data is used to disaggregate AWAP rainfall to 3-hourly values for periods before 1 Jan 2020 and IMERG (<https://gpm.nasa.gov/data/imer>) dataset after 1 January 2020. The 3-hourly to 1-hourly disaggregation is carried out using a method which is part of the JULES modelling framework and involves randomly assigning the start time of the precipitation event throughout the period between the beginning and end of the 3-hour window. Also, the proportion of the timesteps within the 3 hours are randomly selected to be wet, and the precipitation is distributed uniformly among them (Williams and Clark, 2014).

2.2. Live fuel moisture content

The LFMC product used in this study is generated using a radiative transfer model inversion technique on the MODIS reflectance data (Yebra et al., 2018) and publicly available via the Australian Flammability Monitoring System. First, three different radiative transfer models are used to simulate reflectance spectra for the moisture content range for three broad fuel classes (grasslands, shrublands and woodlands/forest). The cropland/agricultural fuel is classified within the grassland fuel class as the vegetation structure of cropland and grassland are similar from a radiative transfer modelling perspective. The MODIS-derived land cover product (MCD12Q1 Collection 5 (Friedl et al., 2010) is used to identify the dominant fuel class corresponding to each pixel and day of interest. The simulated spectra corresponding to that fuel class are then used as reference lookup tables to map the corresponding LFMC values from the quality-controlled observed MCD43A4 Version 6 Nadir Bidirectional Reflectance Distribution Function (BRDF)-Adjusted Reflectance (NBAR) dataset (Strahler et al., 1999) of the same day. The MODIS reflectance and land cover data are at 500 m resolution resulting in LFMC retrievals of 500 m spatial resolution. The algorithm is run every four days as a trade-off for data volume to storage and FMC dynamics. To develop the predictive model, the LFMC data (500m) was upscaled to JASMIN's 5 km resolution by taking an average of the LFMC values that are encompassed within each JASMIN pixel.

2.3. Fire radiative power

Fire Radiative Power (FRP) estimates are available from the MCD14ML standard quality data product (Giglio et al., 2016) and were obtained from the Fire Information for Resource Management System (FIRMS). The MODIS FRP retrieval is based on the relationship between the emitted fire energy and infrared brightness temperature estimates in the 4 μm region (Kaufman et al., 1998). The FRP is provided as a vector product where each of the latitude and longitude values corresponding to an FRP value represents the centre of the 1 km fire pixel. This may not necessarily match the actual location of the fire as one or more fires can be detected within the 1 km pixel. The FRP data and location information is derived from the swath products of MOD14 and MYD14 using the Fire and Thermal Anomalies algorithm (Giglio et al., 2016). The daytime global commission error (false alarm) for this product was found to be 1.2% (Giglio et al., 2016). The FRP is given in a unit of megawatts (MW) per pixel.

2.4. MODIS land use/land cover for data analysis

To evaluate the three gridded products explored in the present study (i.e., AFMS-LFMC, JASMIN SM and predicted LFMC) over various land cover types typical of Australia, a land cover dataset at 0.5 km resolution and based on MODIS Land Cover Type (MCD12Q1) product (Broxton et al., 2014) is used. This dataset provides a more detailed, commonly used, and well-known International Geosphere-Biosphere Program land cover classification than the broader vegetation classifications used in the LFMC algorithm (four fuel types; see section 2.2) or in JULES/JASMIN (5 plant functional types; Best et al., 2011). The MODIS data defines 13 dominant vegetation types and can help to characterize the LFMC and SM products over a variety of land cover types. The MODIS land cover data is derived by weighting each land cover type by its corresponding confidence score for each year and using the highest-weighted land cover type in each pixel in the 2001–2010 MCD12Q1 data (Broxton et al., 2014). The MCD12Q1 dataset form the basis of the dominant fuel classification used in the AFMS-LFMC algorithm (Yebra et al., 2018). This land cover data is found to be better than the Global Land Cover Characteristics database, which is based on 1 year of Advanced Very High Resolution Radiometer (AVHRR) data (Broxton et al., 2014).

2.5. Study period

The data used in the present study covers January 2010 to June 2020 period. 2010-2020 is a period with large inter-annual variability in precipitation over Australia, 2010 and 2019 being the wettest and driest years on record, respectively. The 2019-20 fire season (spring-summer period) witnessed large scale fire events in Australia and burned an estimated 186,000 square kilometres of land. It is estimated that the 2019/20 forest fires have burned 21% of the Australian temperate broadleaf and mixed forest biomes until early January 2020 (Boer et al., 2020). Sampling the inter-annual variability correctly is important when constructing the model. At the same time, having a large enough test sample is imperative to yield statistically meaningful results. The data covering 2010 – 2011 and 2013 - 2019 is used as the training dataset to construct the model. The model predictions were verified over 18 months, for the whole of 2012 and from January – June 2020, which falls outside the training data period. The year 2012 is one of the "normal" years (close to the long-term average) among the years considered here. Rainfall for 2020, until autumn, was below average for Australia as a whole, although there are marked differences in results across the nation (Bureau of Meteorology climate statements available from <http://www.bom.gov.au/climate>).

3. Methodology

3.1. Analysis of the relationships between SM and LFMC

The relationship between SM and LFMC were first evaluated at 60 selected locations over three well-known SM networks, named CosmOz, OzFlux and OzNet from 2010-2019 (Fig. 1). The 60 locations sample the climatic zones and vegetation types typical of the Australian landscape. JASMIN has also good skill at these sites (Vinodkumar and Dharssi, 2019). The strength of the relationship was analysed using the lag-correlation. The data at each location was obtained by collocating the 5 km LFMC and SM grids using the nearest-neighbour approach.

A normalized SM field is used where JASMIN is compared against the MODIS FRP values. The normalisation scales the volumetric data between (0, 1) using the minimum and maximum values from the respective time series. Thus, the normalisation gives a "relative" SM field which represents the "fraction of full wetness" and is often simply called soil wetness (SW) in the literature (Dharssi and Vinodkumar, 2017). It is worth noting that the applied normalisation is a linear transformation and hence the transformation does not affect the correlations computed. We selected soil wetness in this analysis against FRP as it is a better

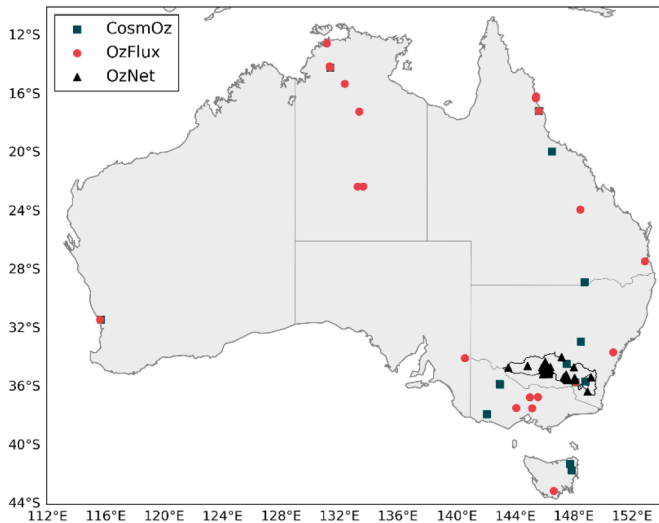


Fig. 1. Study sites. The locations correspond to the three in situ SM networks - CosmOz, OzFlux and OzNet.

indicator of wet and dry conditions than the volumetric SM. The latter is controlled by the static soil properties (i.e., field capacity and wilting point) which is found to have large spatial variability. The evaluation against FRP was carried out for the training period (2010-2011 and 2013-2019 combined). The land cover classification was made based on the 500 m resolution MODIS land cover land use type dataset (Broxton et al., 2014). Low-intensity fire pixels (FRP < 50 MW) were omitted for the analysis as these constituted a disproportionately large portion (~63%) of the total sample size and can dominate the sampling variability.

3.2. LFMC predictive model

A modelling strategy similar to that discussed in Fovell et al. (2015) was adopted in the present study, where it is hypothesised that daily variations in LFMC from its annual cycle can be predicted using daily deviations from the annual cycle in SM. The annual model for both LFMC and SM is based on a Fourier cosine series approximated to the 12th harmonics, where day-of-the-year is used as the predictor variable. The daily changes in LFMC were computed using an ordinary least square regression model with the lagged, residual (deviation from the annual mean) SM as the independent variable. The predictive model can be written as:

$$LFMC = \alpha + \sum_{n=1}^{12} \beta_n \cos\left(n \frac{\pi D}{L}\right) + \gamma' SM_{lag} \quad (1)$$

The ' α ' term represents the first coefficient of the Fourier series and the intercept of the ordinary least square regression model combined. ' β ' is the leading coefficient for the cosine waves in the Fourier series and ' γ' is the slope of the ordinary least square regression model, D is the day of the year, L is the total number of days in a year (approximated to 366) and SM_{lag} is the lagged, daily SM deviations from its annual cycle.

The model parameters change with location (grid points) except for the lag. A constant lag of 14 days was selected which helps to keep the predictive model simple without penalizing the model skill. The deliberation for the model structure and the choice of lag value is discussed in the results and discussion section (4.3). As discussed in Section 3.1, the model is initially developed at each site in the three soil moisture networks. Subsequently, the predictive model is calibrated for each JASMIN grid point and thus allowing to predict LFMC at 5 km spatial resolution.

3.3. Evaluation metrics

Pearson's product-moment correlation (r), normalised root mean square difference (NRMSE) and bias scores were used to evaluate the results. NRMSE is defined as the root mean square difference normalised using the range of the reference dataset. The scores are computed for all locations and the period for which the comparing data overlaps. Only significant correlations (p -values < 0.05) are presented. The equations for each of the above-mentioned metrics are given below.

$$r = \frac{\frac{1}{N} \sum_{i=1}^N (X - \bar{X})(Y - \bar{Y})}{\sigma_X \sigma_Y} \quad (2)$$

$$NRMSE = \frac{\sqrt{\frac{1}{N} \sum_{i=1}^N (X - Y)^2}}{\max(X) - \min(X)} \quad (3)$$

$$Bias = \frac{1}{N} \sum_{i=1}^N (X - Y) \quad (4)$$

where X and Y are the variables evaluated. Lag-correlation is primarily used to identify the strength of the relationship between SM and LFMC. In this case, X in Eq. (2) is the LFMC time series shifted by n days, where n is lag in days. When the model predictions are evaluated, X and Y are AFMS-LFMC and predicted LFMC, respectively. " σ " is the standard deviation. Fisher's transform is applied to calculate the average and median correlation (Corey et al., 1998).

4. Results and discussions

4.1. Relationships between SM and LFMC

LFMC generally displays a strong seasonality where the values typically reach their lowest before the seasonal rains have commenced. This seasonal cycle is illustrated through the time series plot over Baldry in the southern tableland region of New South Wales (black, dotted line; Fig. 2). The Baldry site is part of the CosmOz network with the land classified as a mix of pasture and reforested woodland. The site is situated in a semi-arid environment with annual rainfall dominated by winter precipitation produced by mesoscale extra-tropical disturbances. The LFMC time series over Baldry shows peaks after the wet season and the vegetation gradually drying out into the drier summer months. The site also displays short-lived spikes after significant rain events, highlighting that the plants can utilise moisture transported into the shallow soil layers after a rain event.

JASMIN has four soil layers, and it is not precisely clear which of these layers best represents the root zone at a given location. The top two layers are often found to be influenced by weather events characterised by sharp wetting and drying phases. The temporal dynamics of these two layers at Baldry typify the widely occurring pattern across the sites. Temporal variations in the 35-100 cm layer are less sizable and rather smooth compared to the two layers over it. This layer is less influenced directly by what happens at the surface as the top two layers act as a natural filter in modulating the water transport downwards. The bottom-most soil layer in JASMIN is even less dynamic due to the depth and thickness of the layer. In general, the bottom two layers show similar temporal characteristics across locations as well. There is a visible hysteresis and only the significant and persistent rain events recharge the bottom layers.

To identify the strength of a linear relationship that may exist between SM and LFMC, a lag-correlation analysis was conducted between AFMS-LFMC and SM. All the native JASMIN layers (0-10 cm, 10-35 cm, 35-100 cm, 100-300 cm), as well as the various combination of layers (i.e., 0-35 cm, 0-100 cm, 0-300 cm, 10-100cm, 10-300cm, 35-300 cm) that can be derived using the four native soil profiles (using a weighted average based on layer depth), is used for the lag-correlation analysis.

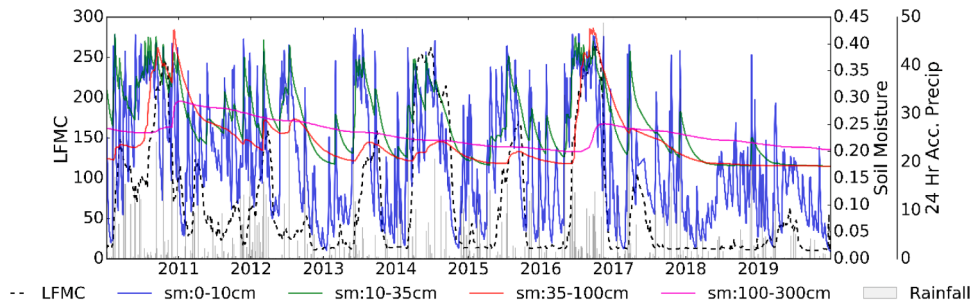


Fig. 2. Time series plots of LFMC, SM and 24-hour accumulated rainfall over the Baldry site in New South Wales. LFMC (%) data is from the AFMS, SM ($\text{m}^3 \text{m}^{-3}$) from the JASMIN and rainfall (mm) from the AWAP.

The results presented in Fig. 3 depict the box and whisker plot generated using the maximum lag-correlation and the corresponding lag (in days) obtained at each site. The skill scores are segregated into four broad land use-land cover (LULC) types. The land cover classification is made based on the information from *in-situ* locations. The results indicate that the strength of the relationship between LFMC and SM generally varies from site to site. The observed variation in the correlation can be caused by a variety of factors, including spatial variability in plant type, physiology and morphology, climate, soil properties and depth. The range in lag time indicates that there is a significant difference in the physical processes happening at each location, from the transport of water through the soil from the surface to the root-zone and the eventual uptake of moisture by plants.

From the analysis, we identify SM content from the 0-35 cm profile ($\text{SM}_{0-35\text{cm}}$) provides the best skill in terms of the correlation with LFMC. Interestingly, studies using measured soil moisture over various locations in Oklahoma, USA, found that 0-40cm profile soil moisture are a good indicator of LFMC (Kruger et al., 2017; Sharma et al., 2020). This result is consistent with what we have observed and validates our finding that moisture in topmost soil layers can be a good indicator for LFMC changes. The $\text{SM}_{0-35\text{cm}}$ displays a strong relationship with the LFMC at different land cover types. One possible reason for this larger degree of agreement is that both the $\text{SM}_{0-35\text{cm}}$ and LFMC exhibits strong seasonality. The deeper layers may not always display the strong seasonality exhibited by the shallower layers. Besides, the deeper layers may miss the short-term variations associated with individual weather events to which the plants and shallow soil profiles respond. Also, the upper and deeper soil layers can be disconnected in land surface models due to uncertainties in the parameterisations. This may result in deeper layers exhibiting little seasonality, rendering them less useful to predict

seasonal LFMC changes. This also gives rise to artificial correlations at a longer time lag, as evident from the box and whisker plots for the 100-300 cm profile (Fig. 3). A longer lag is generally observed for all soil layer over the forested sites. The reasons for this behaviour are not understood and cannot be explored without additional information on the complex processes that govern SM and LFMC dynamics over these locations. It may be due to the slow infiltration rate and/or the prevalence of root water uptake from deeper soil horizons in these forest biomes. However, it is to be noted that the variability in the median lag between different soil layer is low over forested sites and which may invalidate this argument. Future studies may need to explore this further. The other possibility, as mentioned above, is that the long lags correspond to artificial correlations that are non-physical.

In general, a strong linear relationship ($R>0.5$) is found between the LFMC and $\text{SM}_{0-35\text{cm}}$, except for forested locations (Fig. 3). The correlation and corresponding lag between LFMC and $\text{SM}_{0-35\text{cm}}$ is segregated based on four broad land use-land cover (LULC) types, i.e., grasslands, woodlands, forest, and croplands. The north Australian savannahs, temperate woodlands etc are classified as woodlands where the trees are scattered and sparse. All pasture and grazing paddocks are included under grasslands. Forest class represent densely vegetated trees and comprises tropical and temperate rainforests, boreal forests etc. The land cover classification is made based on the information from *in-situ* locations. For each LULC type, then mean and median correlation and lag are calculated. The mean (median) obtained for grasslands, woodlands, forest, and croplands are 0.73 (0.74), 0.69 (0.64), 0.43 (0.43) and 0.57 (0.51), respectively. The corresponding average (median) lag is 13 (13), 65 (5), 220 (290) and 20 (26) days. The average lag discussed above and in the following discussions are rounded to the nearest integer. The forested sites generally display a stronger correlation to the thicker, 0-

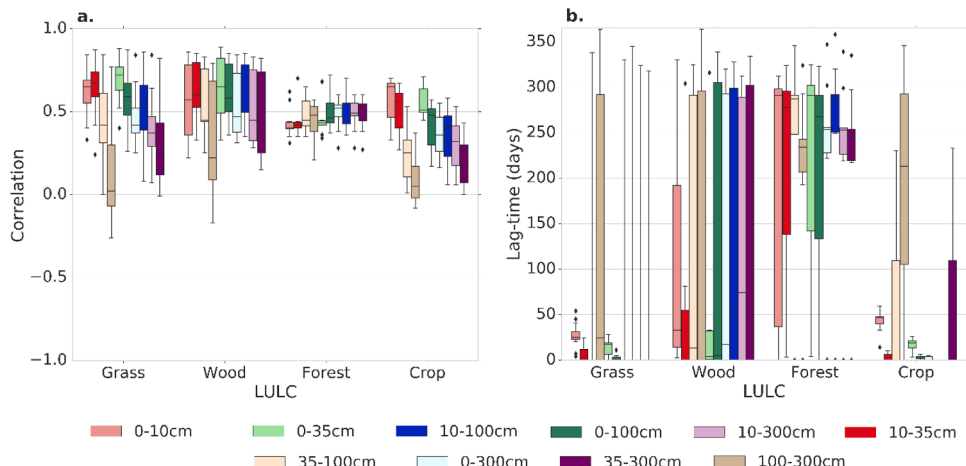


Fig. 3. Box and whisker plot representing a) the highest lag-correlation obtained and b) the corresponding lag in days between AFMS-LFMC and SM from various JASMIN native (0-10 cm, 10-35 cm, 35-100 cm, 100-300 cm) and derived (0-35 cm, 0-100 cm, 0-300 cm, 10-100cm, 10-300cm, 35-300 cm) layers. The grouping is done based on the LULC type of the observing site. The outliers are marked as diamonds.

300 cm soil profile. This is likely a consequence of the deeper roots typical of over-story forest canopies which can draw water from a much thicker soil profile than the 0–35 cm layer. Also, additional uncertainties may exist in both SM and LFMC calculations over forested sites due to limitations in the estimation techniques owing to lack of process representation, inaccurate parameterization, or uncertainties in driving data. The skill lost by using the 0–35 cm profile instead of the 0–300 cm, in terms of the difference in mean (median) correlation, is 0.05 (0.02).

4.2. Comparison of SM_{0-35cm} and LFMC over fire events

The association of SM_{0-35cm} to LFMC exhibit very different behaviour for different land cover types as indicated by the correlation analysis. This is further explored in the context of fire activity using the MODIS FRP data. The land cover type corresponding to the MODIS FRP pixel is identified using the MODIS LULC dataset described in Section 2.5. The LULC class, SM_{0-35cm} , and LFMC grid point values nearest to the FRP data location is selected for the analysis. Fig. 4 illustrates the probability distribution of normalised SM_{0-35cm} (SW) and LFMC for grassland and evergreen broadleaf forest land cover types over locations and periods where a fire was detected according to MODIS FRP (Fig. 4).

Over grasslands, 98% of fire occurs when the SW is ≤ 0.5 (Fig. 4a). Some of the highest FRP values (≥ 1000 MW) corresponds to very dry soils ($SW < 0.25$). Analysing the LFMC over fire occurrences, ~95% of fires occur over grasslands when the LFMC is $<100\%$ (Fig. 4b). The relationship is found to be more complicated for the evergreen forest sites (Fig. 4c). Here, about 10 % more fires are found to occur over wetter soils ($SW > 0.5$) compared to grasslands (Fig. 4c). The drier soils under grassland, compared to the forest, may reflect the fact that the water uptake in grasses occurs from shallow soil layers and is also higher than that in woody vegetation (Köchy and Wilson 2000). This is facilitated by higher (~20 times) fine root lengths in grassland soils than in forest soils (Jackson et al. 1997). Besides, the root-shoot ratio is nearly 30 times greater in grassland than forest (Wilson 1993).

Similar to grassland, the most intense fires ($FRP > 1000$ MW) over evergreen broadleaf forests are found to occur when $SW < 0.5$ (Fig. 4c). These forested trees can hold water equivalent to its dry weight, even during periods conducive to fires. This is evident from the frequency distribution of LFMC where a large proportion of fires occur when LFMC is around 100% (Fig. 4b). The LFMC at these sites seldom falls below 50% in the event of a fire occurring (Fig. 4d). The evergreen trees are found to have high wood density and hence can store a substantial

amount of water in the stem (Kenzo et al., 2017). Also, the development of deep roots and subsequent water uptake from deeper soil layers are found to be an important strategy enabling evergreen species to overcome seasonal water limitations (Hasselquist et al., 2010). The average root depth in evergreen forests is estimated to be about 3.1 m (Yang et al., 2016). The low correlations observed over forested sites (Fig. 3a) is possibly a result of these drought-resistant strategies adopted by the particular vegetation types.

It is worth noting that the findings from this analysis, which identified that wildfires occur predominantly over the landscape at low soil moisture conditions, is comparable to studies done in other parts of the globe. For example, Krueger et al (2015) studied growing season fires in Oklahoma, USA, where they observed that 91% of large fires (≥ 121 ha) occurred when the fraction of soil water (synonymous to SW) was < 0.5 . Further, an observational study conducted by Sharma et al (2020) over tallgrass prairie sites in Oklahoma, USA, observed that the live fuel moisture over these biomes were $< 120\%$ when $SW < 0.5$. This, again, is consistent with what observed over Australian grasslands, where LFMC is generally $< 100\%$ during fire occurrences and more or less coincide with dry soil moisture ($SW < 0.5$) conditions.

4.3. Development of the LFMC predictive model at point locations

The differentiable distribution of LFMC among various vegetation type and also with the SM, as demonstrated in Fig. 4, highlights the complexity and the variability of physical processes that modulates the LFMC dynamics. This also, possibly, explains the somewhat different mean annual cycles exhibited by LFMC to SM (Fig. 5). It is quite obvious from Fig. 5 that the LFMC and SM displays different annual cycles. This is true for all 60 sites analysed (not shown here for brevity). The mean annual cycle of SM and LFMC is calculated using the respective datasets available for the 2010–20 period. The temporal variation in LFMC is influenced by the plant eco-physiological processes linked to both water and carbon cycle. The processes related to the water cycle that can influence LFMC includes SM availability, soil water uptake, plant water storage, and water loss through transpiration (Jolly and Thompson, 2018). Thus, SM is only one of the many factors that can modulate LFMC. SM is likely a proxy for the change in plant water status, and hence a proxy for changes in the numerator for LFMC definition (i.e., wet weight). The carbon cycle processes are found to influence the change in dry weight of the vegetation, i.e., the denominator in LFMC formulation (Jolly and Thompson, 2018). Studies have shown that

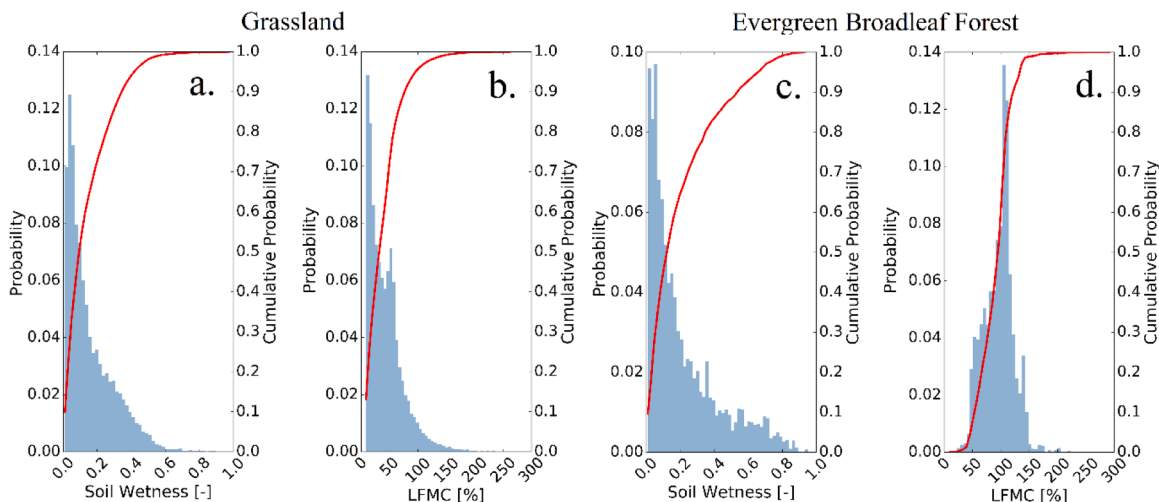


Fig. 4. Probability (bar plot) and cumulative probability (red line) distribution of soil wetness (SW) from 0–35cm profile and LFMC over grasslands (a and b), and evergreen broadleaf forests (c and d). Each data point corresponds to the location identified as fire hotspots by the MODIS FRP data covering the whole of Australia. SW is defined as the “fraction of full wetness” and is derived by scaling the volumetric SM time series of interest (SM_{0-35cm}) using their minimum and maximum values. The resulting soil wetness range between (0, 1), where 0 mean “driest” and 1 means “wettest”.

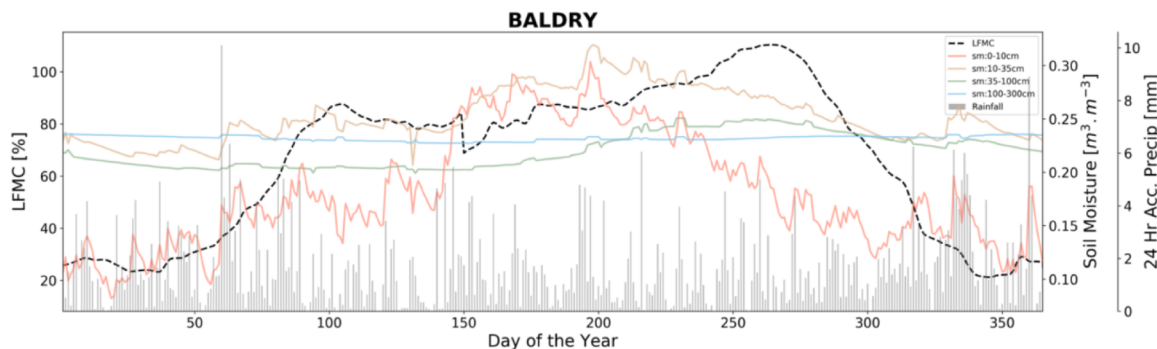


Fig. 5. Mean annual cycles of LFMC (broken black line) and SM (coloured lines) over Baldry in the state of New South Wales, Australia (coordinates: 32.8710°S, 148.5260°E). The grey bar indicates the mean 24-hour accumulated precipitation from the AWAP daily gridded rainfall analysis. Baldry site is a mix of pasture and reforested woodland. The annual mean is computed using the data from January 2010 to June 2020.

changes to dry matter exert a stronger control on seasonal LFMC dynamics than actual changes in water content (Jolly et al., 2014). Most of these parameter datasets are not readily available and has to be captured in the model to derive a skilful LFMC product. The sub-model to capture the annual cycle, thus, implicitly addresses the factors that influence the LFMC seasonal dynamics.

For a sufficiently long time series, the annual cycle can be computed by just taking the daily climatological mean. This is not possible here due to the shorter time series only covering 10 years, with significant interannual variability within. Further, the AFMS-LFMC product has a coarser temporal resolution (4 days) and the frequency can be affected by the presence of cloud cover. The annual cycle of both LFMC and SM varies from location to location, and hence each site requires a unique model. The Fourier cosine series approximated to the 12th harmonics (Eq. 1) is found to be capable of estimating fairly odd-shaped annual cycles in both datasets, an example of which is shown in Fig. 6 for the Tumbarumba wet-sclerophyll site in New South Wales.

Based on the analysis in Sections 4.1 and 4.2, the SM content from the 0–35 cm profile (SM_{0-35cm}) is found to be a good predictor for LFMC and was used in the present study to model the LFMC. The selection of a single SM profile satisfies our immediate goal of developing a simple yet skilful model for predicting LFMC using a SM product. When the AFMS-LFMC time series is compared to the annual model for the full data period, a sizable 51.8% of the reference series' variance is captured by the annual model, where the value represents the average for the 60 stations examined (see Supplementary Table 1). Similarly, for the SM_{0-35cm} , the average variance that can be explained by the annual model is found to be 44.8%. The SM_{0-35cm} departures are generally found to have

good agreement with the LFMC departures. This is illustrated in Fig. 7, where a direct comparison is facilitated by superimposing the two residual time series over the Whroo site in the northern parts of the state of Victoria (Coordinates: 36.6732°S, 145.0294°E). However, a systematic phase difference between the two residual time series over the Whroo site is found (Fig. 7). The SM_{0-35cm} departures are generally found to lead the LFMC departures with a systematic phase difference existing between the two residual time series. The lag and the strength of association between the two residual time series is found to vary from location to location (Fig. 8). The mean (median) lag for grassland, woodland, forestland, and cropland are 14 (14), 15 (0), 10 (0) and 12 (16) respectively (Fig. 8). The corresponding lag-correlation values are 0.65 (0.65), 0.42 (0.45), 0.27 (0.25), and 0.55 (0.56). The extremely short lag over a few of the forestland and woodland sites can be anomalous and may indicate a data representativeness issue. The site averaged (median) lag obtained was 13 (14) days. This result further suggests that LFMC is responding directly and strongly to SM_{0-35cm} changes and the lag signifies the combined time taken for the rainfall received at the surface to percolate through the 0–35 cm layer and the subsequent water uptake process by the plant to occur.

The daily departures of the 14-day lagged SM_{0-35cm} is found to provide a reasonable linear relationship with the LFMC residual time series at all locations and was selected to construct the model. The daily deviations in LFMC were thus predicted using that in 14-day lagged SM_{0-35cm} , where the daily departures were calculated by removing the respective annual cycles from each dataset. A constant lag of 14-days helps to keep the predictive model simple. The annual cycle was calculated using the Fourier based model described above and in Eq. 1.

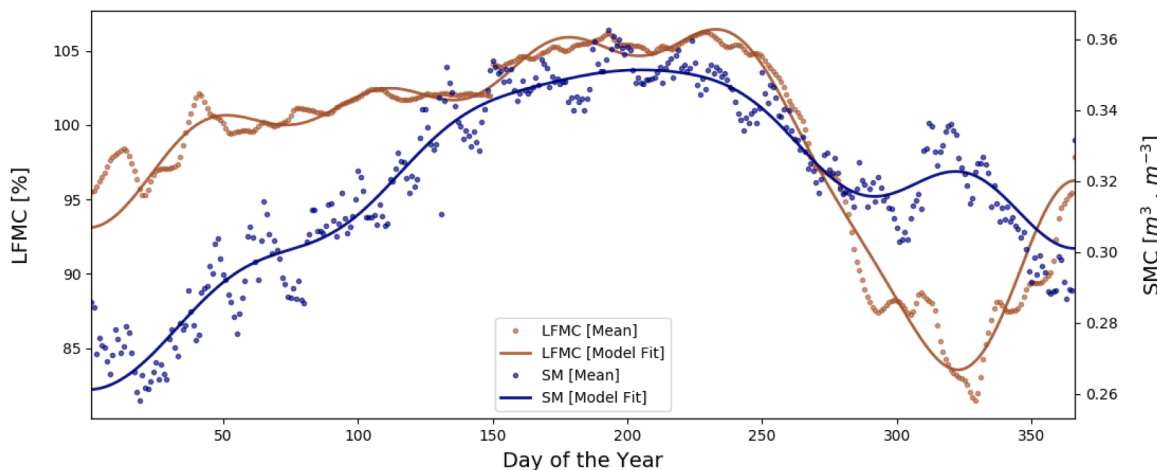


Fig. 6. Observed (dotted lines) and modelled (continuous line) annual cycles over Tumbarumba, New South Wales (coordinates: 35.6566°S, 148.1517°E) for LFMC (brown line) and SM_{0-35cm} (blue line). The Tumbarumba site is located in the wet sclerophyll, Bago State forest in south-eastern New South Wales.

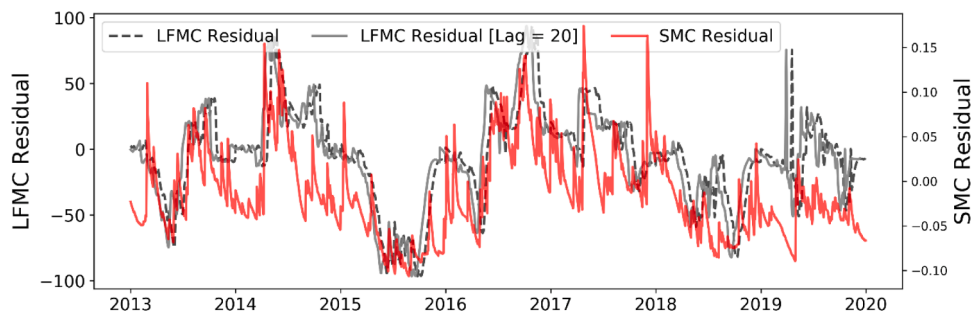


Fig. 7. Residual (departure from the annual cycle) time series of SM_{0-35cm} (red line) and LFMC (black broken line) over Whroo in the northern parts of the state of Victoria (coordinates: $36.6732^{\circ}S$, $145.0294^{\circ}E$). The grey solid line corresponding to the LFMC shifted backward for 20 days. The Whroo site is classified as a box woodland ecosystem.

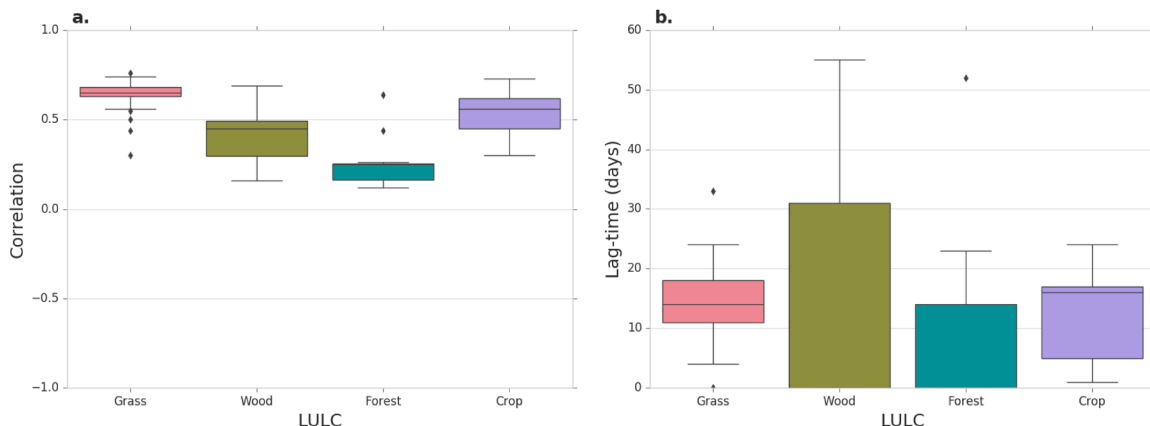


Fig. 8. Box and whisker plot representing a) the highest lag-correlation obtained and b) the corresponding lag in days obtained between residual time series of LFMC and SM_{0-35cm} for different LULC types. The grouping is done based on the LULC type of the observing site. The outliers are marked as diamonds.

Separate ordinary least square regression models with the residual 14-day lagged SM_{0-35cm} as the independent variable to predict daily changes in LFMC was developed for each location. The final predictive model was thus constructed using a linear combination of two sub-models - the Fourier series-based model to predict the annual cycle and the ordinary least square regression model to estimate the daily variations. As mentioned earlier, the model parameters were computed for each grid point due to the spatial variability in LFMC and SM.

The predictive model returned an average R^2 of 0.70 and an RMSD of 14.1% over the 60 sites for the training period. The fit varies with

location and the R^2 obtained ranges from 0.21 to 0.89. There are only 11 sites with an $R^2 < 0.5$ out of the total 60. This is quite encouraging given the simplicity of the modelling approach used here. A variety of reasons could cause the lack of fit observed at a specific location including, but not limited to, data representativity, LFMC and SM model parameter uncertainty, driving and ancillary data errors, and LFMC and SM model physics limitations. An example of a site where the model fit is reasonably good is the Cumberland Plain site ($33.6152^{\circ}S$, $150.7236^{\circ}E$) in central New South Wales (Fig. 9a). The Cumberland Plain site is located in a dry sclerophyll forest at an elevation of 20 m above mean sea level.

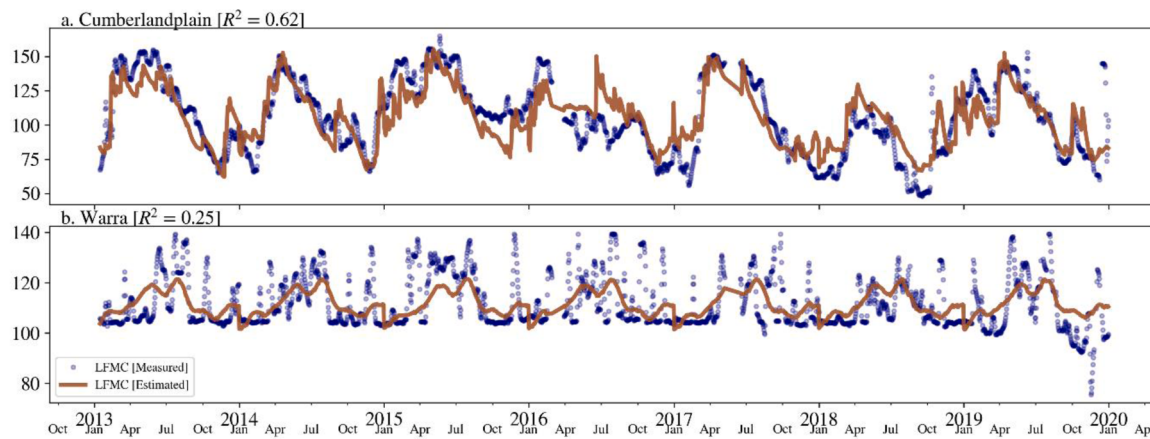


Fig. 9. Time series of modelled (light red line) and AFMC (black dots) LFMC over Cumberland Plain and Warra sites. The Cumberland Plain station located in dry sclerophyll forest in the Hawkesbury Valley in central New South Wales. The Warra site is located in a wet Eucalyptus forest and is situated in a temperate climate zone in southern Tasmania.

The model handles well both the increasing and declining phases in LFMC related to both seasonal and short-term variations over the Cumberland Plain site. The R^2 obtained at this site is 0.62 with an NRMSD of 13%. The mean \pm standard deviation obtained from the AFMS-LFMC time series over Cumberland Plain is $108.26\% \pm 25\%$. The corresponding value for the predictive model is $107.99\% \pm 19.87\%$.

One of the locations where there is a distinct lack of fit between the modelled and AFMS-LFMC is over the Warra site (coordinates: $43.0950^\circ S, 146.6545^\circ E$) in southern Tasmania (Fig. 9b). The Warra site is located in a wet Eucalyptus forest and is situated in a temperate climate zone. The R^2 and NRMSD obtained over Warra are 0.25 and 13.2%, respectively. The sample mean \pm standard deviation values for AFMS and modelled LFMC are $111.45\% \pm 9.71\%$ and $111.5\% \pm 4.83\%$, respectively. That is, the variance in the AFMS-LFMC is about 4 times that in the modelled one. A repercussion of this high noise in the AFMS-LFMC dataset is that it can influence the quality of the annual cycle estimated by the model. It is observed that the sites where the AFMS LFMC are very noisy have a poor model fit. In the case of Warra, the annual model could only capture 24% variance in the AFMS-LFMC time series. Compared to this, the annual model over Cumberland Plains captured 36% of the variance in the AFMS-LFMC time series. Further, on the wetter side of the distribution (i.e., first quadrant of the residual scatter plot), the AFMS-LFMC shows larger variability than the SM (see Supplementary Figure 1). This possibly highlights controls on daily LFMC dynamics other than the SM in the 0–35 cm profile and which is not represented here. Hence, the specified linear relationship may not be adequate to capture these variations seen in residual LFMC. It is also worth noting that Warra is one of the sites where the JASMIN SM has a low skill (Vinodkumar and Dharssi, 2019). Hence, a combination of factors may have contributed to the bad fit over Warra.

4.4. Training period: Model fit over the 5 km grid

The calibrated LFMC predictive model is applied to the whole of Australia. A strong correlation is observed over the tropical, northern savannas and southern grasslands and croplands (Fig. 10a). The model is found to be generally unbiased (see Supplementary Figure 2 for details). The random error in the model is usually less than 25% of the dynamic range as indicated by the NRMSD score (Fig. 10b).

The evaluation of the model for training period is extended by comparing the AFMS-LFMC and modelled LFMC against the MODIS FRP data are presented in Fig. 11 for four land-cover types identified using the MODIS LULC data. A \log_{10} transformation is applied to the FRP data. For the original AFMS dataset, the mean and standard deviation of LFMC over grassland, cropland, woody savannas, and evergreen broadleaf forests when a fire is detected (using MODIS FRP data) are $41.8 \pm 30.8\%$,

$76.6 \pm 33.6\%$, $54.3 \pm 14.3\%$, and $93.2 \pm 26.5\%$, respectively. The corresponding scores from the predictive model are $49.9 \pm 29.6\%$, $86.1 \pm 25.9\%$, $58.5 \pm 13.1\%$, and $93.1 \pm 19.3\%$, respectively. The model is found to generally capture well the distribution of the original, AFMS-LFMC product. The model fit over woody savannas (Fig. 11b) and evergreen broadleaf forests (Fig. 11d) is found to be particularly good. These biomes exhibit a clear and consistent annual cycle which is captured well by the model. This is evident from the good annual model fit (in terms of R^2) observed over the sites that characterize these LULC types (Table 1). Tumbarumba and Cape Tribulation are examples for evergreen broadleaf forests that shows good annual model fit. Daly and Dry River sites are examples for woody savannas (see <http://www.ozflux.org.au/monitoringsites> for respective site descriptions).

4.5. Validation period: LFMC predictive model skill

Fig. 12 depicts the temporal correlation and NRMD obtained from this verification. Only locations with correlations with p -values <0.05 are shown. The predicted LFMC shows a strong correlation in general and especially over the seasonal grasslands and croplands of southern Australia and the northern tropical savannas. There are, however, regions that display weaker correlation. This is quite noticeable over the evergreen forest across the south-eastern Australia where the model is found to have low skill. Weaker correlations are also observed over regions classified as open shrubland typical of central and north-western Australia. The number of temporal data points used to calculate the statistics varies with location and the maximum sample size available is 130. We acknowledge that this is probably a small sample size to derive spatially consistent skill score. The trade-off is to reduce the training period from 8 years which may lead to a less optimal model fit and hence undesirable. However, this leaves us with a limited sample size for verification. To overcome the limited sample size, we applied the percentile bootstrap method to estimate the correlation confidence interval (Johnson, 2001). The data was resampled with replacement and the bootstrapping repeated 1500 times. The resultant 95% confidence interval (CI) for correlation (i.e., 2.5th and the 97.5th percentiles) is presented as the supplementary Figure 3. The results confirm what is already observed in the correlation results provided in Fig. 12a. A strong correlation and shorter CI are observed over regions where there is high vegetation density. Over drier inland regions, the model is found to have low skill evidenced by the low or even negative correlations observed within the CI. These locations are found to have very sparse vegetation with very low to little temporal variability. The Fourier series based annual model is found to overestimate the annual LFMC values and introduces higher temporal variability in the estimates resulting in low correlations. This issue needs to be addressed in future model

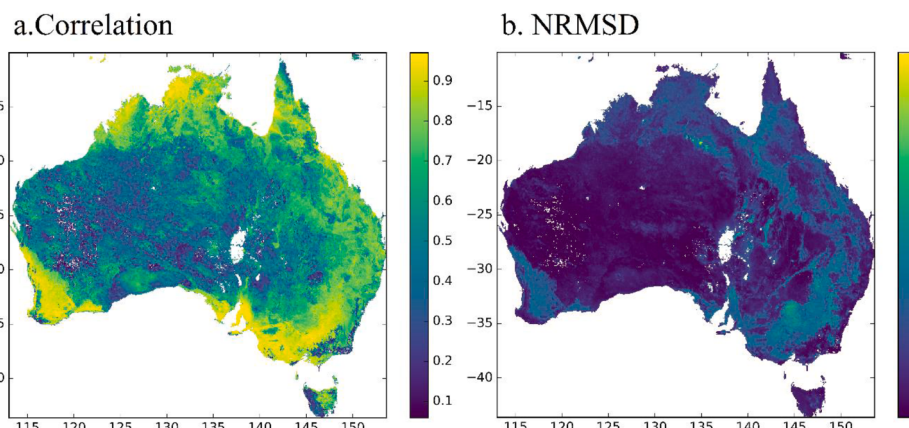


Fig. 10. Pearson's product-moment correlation and NRMSD between the AFMS-LFMC and the predicted LFMC datasets for the training period. Correlations are presented only for locations where p -value <0.05 . The locations where p -value >0.05 is masked in the NRMSD plot as well.

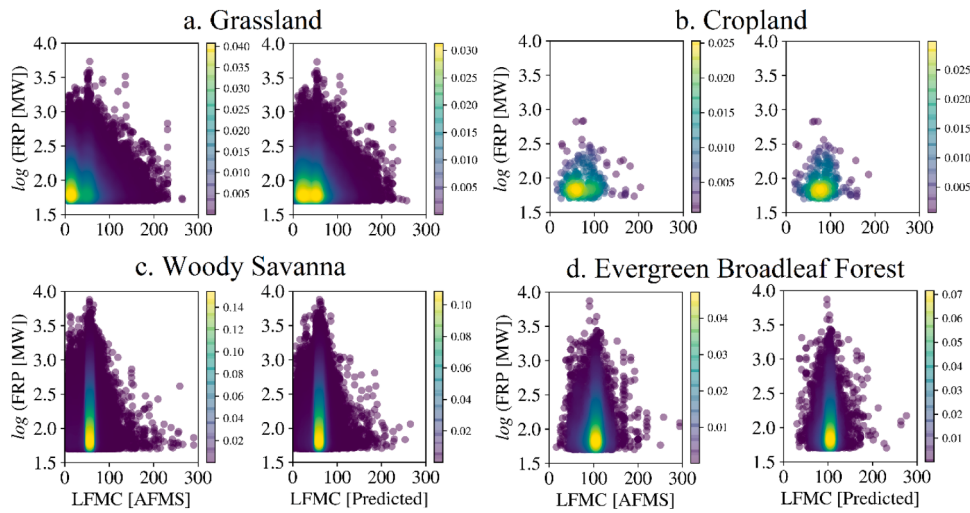


Fig. 11. Scatter plot of AFMS-LFMC and predicted LFMC against the MODIS FRP. The colours depict the probability density estimated using Gaussian kernel density estimation method.

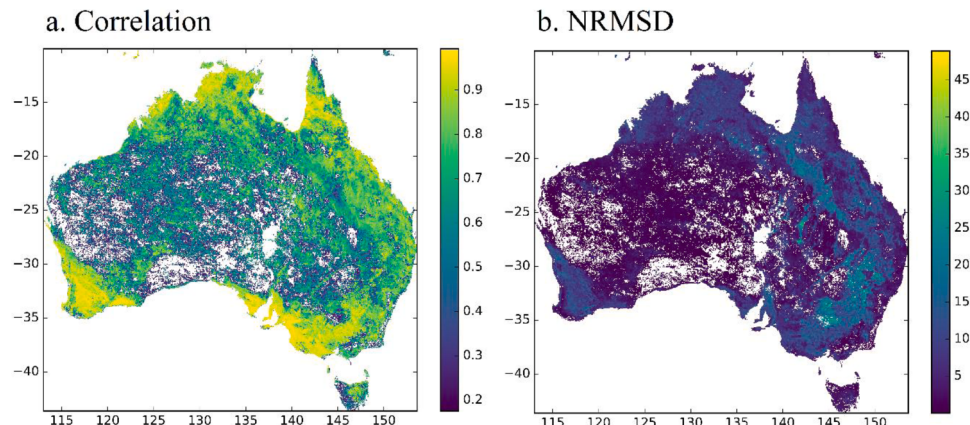


Fig. 12. Pearson's product-moment correlation between the AFMS-LFMC and the predicted LFMC datasets for the test period. Scores are presented only for locations where p -value < 0.05.

development. However, the low correlations generally occur over uninhabited areas with sparse vegetation (mainly shrubs) and low fire risk. Hence, in an operational context, this is not of a big concern.

5. Conclusion

LFMC and SM are widely used in fire management practices - directly and as a proxy for fuel moisture availability, respectively. However, the two variables represent landscape dryness at different strata and the latter can be a good indicator of the former.

This study makes use of readily available gridded LFMC and SM products from the AFMS and JASMIN systems to identify the functional relationship between SM and LFMC. The results indicate that SM is a leading indicator of LFMC. This result has significant operational implications as daily variations in LFMC can be predicted using SM information from JASMIN on a national scale at 5 km spatial resolution, and thereby addressing a limitation of the remote sensing techniques.

This research work aims to advance the understanding of the relationship between the LFMC and SM on a regional scale and sets a forecasting modelling foundation on which future research can build on to provide accurate predictions of LFMC for the whole of Australia. In that respect, the modelling strategy adopted here considers only a single soil profile (i.e., the 0–35 cm profile) from JASMIN and a constant lag value of 14 days at all locations across the country. A lag of 14 days implies a

lead time of 14 days for predicting the LFMC estimates and a maximum lead time of 24 days from a 10-day SM forecast product that is currently available as part of the global numerical weather prediction system. JASMIN is currently run as a prototype, research system with SM analysis done only near-real-time. However, JASMIN can be extended to produce both real-time analysis and forecasts. The prognostic mode could provide SM forecasts for up to 10 days.

Overall, the model fit at most locations is high enough to provide useful information on the timing of LFMC wetting and drying phases for planning fire management operations. This is a significant improvement to the simple temporal and spatial extrapolation of field measurements the fire agencies currently make to estimate LFMC in operational settings. The prediction model is found to have difficulty in capturing the magnitude of sharp wetting phases in LFMC over some locations. Also, the model tends to over predict the dryness at the stations analysed in the point location-based analysis. This, possibly, highlights conditions where the variations in LFMC are not essentially limited to the SM and the systematic, climatological factors alone. Nevertheless, the model is found to provide good accuracy and more importantly captures the dry end of the LFMC spectrum relatively well. This is an important, practical result for the fire danger rating and prediction applications.

The correlation analysis indicates that the dependence of LFMC to SM can vary with vegetation type. For a plant with complex, deeper root systems, the relationship may exist at multiple soil layers. Also, the lag

between the two variables is an attribute of the location determined by a range of factors including soil and vegetation characteristics. Therefore, the future modelling strategy may consider a spatially varying lag as well as a combination of soil layers depending on vegetation type. Another improvement envisaged for the JASMIN system in the future is an upgrade of the SM product from 5 km to 1 km. This will have a subsequent flow-on effect on the resolution of the LFMC product discussed here. A 1 km LFMC product will be beneficial for many operational applications such as planning prescribed burning, where finding moisture content differentials driven by topography is essential.

Noise filtering was not considered as a pre-conditioning step to the construction of the predictive model or in the subsequent estimation here. High-frequency spikes in SM did not match up well with the LFMC data and therefore, a simple, temporal average filter applied to the SM time series may help to improve the correlations between the dataset. The temporal filter applied to a soil profile is similar to expanding the soil horizon downward. At locations where the hydrological coupling between the surface and deeper layers are weak in the model, a temporal filter may help to capture the temporal dynamics of deep layer SM better. However, the time window/parameter(s) for a temporal filter is location specific and should be carefully chosen. The time parameter, in effect, represents all the processes affecting the temporal dynamics of SM, such as the thickness of the soil layer, soil hydraulic properties, evaporation, run-off and vertical gradient of soil properties (texture, density). SM studies have successfully applied an exponential time filter to derive deep layer SM from the near-surface layer SM estimates. Future research may investigate similar methods to address some of the issues arising with the data noise or representative soil depth.

There are other avenues to be explored in the context of using SM information for mapping and predicting LFMC. For example, grassland fires are a major threat in the Australian landscape and grass curing is a well-known indicator of fire potential in grassland ecosystems. Studies have shown that SM exhibit, in general, a strong relationship with grass curing (Sharma et al., 2020). Therefore, the approach discussed in the present study can be extended to identify the relationship between grassland curing and SM. There is rapid progress made in the use of soil moisture and vegetation information to better understand and predict fire danger, particularly on methods that use remote sensing information (e.g., Farahmand et al., 2020, Hyoung 2021, Rigden et al., 2020). The vegetation optical depth (VOD) information retrieved using microwave radiometry measurements is such a product and is found to be a useful indicator of vegetation water content (Konings et al., 2016). A recent study has assimilated VOD from Soil Moisture Active Passive Mission (SMAP) into a coupled dynamic vegetation - land surface model to assess the impact of 2019 Australian fires on regional water budget (Kumar et al., 2020). This study used NASA's Land Information System (LIS) framework to assimilate the SMAP VOD retrievals. Given that there is a proposal to implement JASMIN within NASA's LIS framework, there is an opportunity to further explore the use of VOD information in JASMIN to estimate soil moisture more accurately and in consistent with the vegetation changes associated with fires. Further, assimilation of the VOD data can help to improve the mapping and prediction of the vegetation parameters in the model (e.g., leaf area index) and which can be potentially used in future modelling strategies to predict LFMC.

Declaration of Competing Interest

The authors declare that they have no known competing financial interests or personal relationships that could have appeared to influence the work reported in this paper.

Acknowledgments

The support of the Commonwealth of Australia through the Bushfire and Natural Hazards Cooperative Research Centre program is acknowledged. We thank our colleagues Andrew Frost, Huqiang Zhang,

Simon Louis and Chun-Hsu Su for their helpful comments during the preparation of this manuscript. We also acknowledge NASA for the MODIS products.

Supplementary materials

Supplementary material associated with this article can be found, in the online version, at doi:10.1016/j.agrformet.2021.108503.

References

- Best, M.J., Pryor, M., Clark, D.B., Rooney, G.G., Essery, R.L.H., Menard, C.B., Edwards, J.M., Hendry, M.A., Porson, A., Gedney, N., Mercado, L.M., Sitch, S., Blyth, E., Boucher, O., Cox, P.M., Grimmond, C.S.B., Harding, R.J., 2011. The Joint UK Land Environment Simulator (JULES), model description - Part 1: energy and water fluxes. *Geosci. Model Dev.* 4 (3), 677–699. <https://doi.org/10.5194/gmd-4-677-2011>.
- Boer, M.M., de Dios, V.R., Bradstock, R.A., 2020. Unprecedented burn area of Australian mega fire fires. *Nat. Clim. Change* 10 (3), 171–172.
- Broxton, P.D., Zeng, X., Sulla-Menashe, D., Troch, P.A., 2014. A global land cover climatology using MODIS data. *J. Appl. Meteorol. Climatol.* 53 (6), 1593–1605.
- Castro, F.X., Tudela, A., Sebastià, M.T., 2003. Modeling moisture content in shrubs to predict fire risk in Catalonia (Spain). *Agric. For. Meteorol.* 116 (1–2), 49–59.
- Corey, D.M., Dunlap, W.P., Burke, M.J., 1998. Averaging correlations: Expected values and bias in combined Pearson rs and Fisher's z transformations. *The Journal of general psychology* 125 (3), 245–261.
- Cruz, M.G., Gould, J.S., Alexander, M.E., Sullivan, A.L., McCaw, W.L., Matthews, S., 2015. Empirical-based models for predicting head-fire rate of spread in Australian fuel types. *Australian Forestry* 78 (3), 118–158.
- Dharssi, I., Vinodkumar, 2017. A prototype high-resolution soil moisture analysis system for Australia. *Bureau of Meteorology Research Report*, No. 026.
- Dimitrakopoulos, A.P., Bemmerzouk, A.M., 2003. Predicting live herbaceous moisture content from a seasonal drought index. *Int. J. Biometeorol.* 47, 73–79.
- Farahmand, A., Stavros, E.N., Reager, J.T., Behrang, A., 2020. Introducing Spatially Distributed Fire Danger from Earth Observations (FDEO) Using Satellite-Based Data in the Contiguous United States. *Remote Sens.* 12, 1252.
- Fovell, R.G., Rolinski, T., and Cao, Y., 2015: A simple model for the live fuel moisture of chamise, 5.3, 11th Symposium on Fire and Forest Meteorology, Minneapolis, Minnesota.
- Friedl, M.A., Sulla-Menashe, D., Tan, B., Schneider, A., Ramankutty, N., Sibley, A., Huang, X.M., 2010. MODIS collection 5 global land cover: algorithm refinements and characterization of new datasets. *Remote Sens. Environ.* 114, 168–182.
- Giglio, L., Schroeder, W., Justice, C.O., 2016. The collection 6 MODIS active fire detection algorithm and fire products. *Remote Sens. Environ.* 178, 31–41.
- Glowacki, T., Xia, Y., Steinle, P., 2012. Mesoscale surface analysis system for the Australian domain: design issues, development status, and system validation. *Weather Forecast.* 27, 141–157. <https://doi.org/10.1175/WAF-D-10-05063.1>.
- Hasselquist, N.J., Allen, M.F., Santiago, L.S., 2010. Water relations of evergreen and drought-deciduous trees along a seasonally dry tropical forest. *Oecologia* 164 (4), 881–890. <https://doi.org/10.1007/s00442-010-1725-y>.
- Huffman, G.J., Bolvin, D.T., Nelkin, E.J., Wolff, D.B., Adler, R.F., Gu, G., Hong, Y., Bowman, K.P., Stocker, E.F., 2007. The TRMM Multi-Satellite Precipitation Analysis (TMPA): Quasi-Global, Multiyear, Combined-Sensor Precipitation Estimates at Fine Scales. *J. Hydrometeorol.* 8 (1), 38–55. <https://doi.org/10.1175/JHM560.1>.
- Hyoung, L.J., 2021. Prediction of Large-Scale Wildfires with the Canopy Stress Index Derived from Soil Moisture Active Passive. *IEEE J. Sel. Top. Appl. Earth Observ. Remote Sens.* 14, 2096–2102. <https://doi.org/10.1109/JSTARS.2020.3048067>.
- Jackson, R., Mooney, H.A., Schulze, E.D., 1997. A global budget for fine root biomass, surface area, and nutrient contents. *Proc. Natl. Acad. Sci.* 94 (14), 7362–7366.
- Johnson, R.W., 2001. An introduction to the bootstrap. *Teaching Stat.* 23 (2), 49–54.
- Jolly, W.M., Johnson, D.M., 2018. Pyro-ecophysiology: shifting the paradigm of live wildland fuel research. *Fire* 1 (1), 8.
- Jolly, W.M., Hadlow, A.M., Huguet, K., 2014. De-coupling seasonal changes in water content and dry matter to predict live conifer foliar moisture content. *Int. J. Wildland Fire* 23, 480–489.
- Kaufman, Y.J., Justice, C.O., Flynn, L.P., Kendall, J.D., Prins, E.M., Giglio, L., Setzer, A.W., 1998. Potential global fire monitoring from EOS-MODIS. *J. Geophys. Res.* 103 (D24), 32215–32238.
- Kenzo, T., Sano, M., Yoneda, R., Chann, S., 2017. Comparison of wood density and water content between dry evergreen and dry deciduous forest trees in Central Cambodia. *Jpn. Agric. Res. Q.* 51 (4), 363–374.
- Kidnie, S., Cruz, M.G., Gould, J., Nichols, D., Anderson, W., Bessell, R., 2015. Effects of curing on grassfires: I. Fuel dynamics in a senescing grassland. *Int. J. Wildland Fire* 24, 828–837. <https://doi.org/10.1071/WF14145>.
- Köchy, M., Wilson, S.D., 2000. Competitive effects of shrubs and grasses in prairie. *Oikos* 91 (2), 385–395.
- Konings, A.G., Piles, M., Rötzer, K., McColl, K.A., Chan, S.K., Entekhabi, D., 2016. Vegetation optical depth and scattering albedo retrieval using time series of dual-polarised L-band radiometer observations. *Remote Sens. Environ.* 172, 178–189.
- Krueger, E.S., Ochsner, T.E., Engle, D.M., Carlson, J.D., Twidwell, D., Fuhlendorf, S.D., 2015. Soil Moisture Affects Growing-Season Wildfire Size in the Southern Great Plains. *Soil Sci. Soc. Am. J.* 79, 1567–1576. <https://doi.org/10.2136/sssaj2015.01.0041>.

- Krueger, E.S., Ochsner, T.E., Quiring, S.M., Engle, D.M., Carlson, J.D., Twidwell, D., Fuhlendorf, S.D., 2017. Measured Soil Moisture is a Better Predictor of Large Growing-Season Wildfires than the Keetch–Byram Drought Index. *Soil Sci. Soc. Am. J.* 81, 490–502. <https://doi.org/10.2136/sssaj2017.01.0003>.
- Kumar, S.V., Holmes, T., Andela, N., Dharssi, I., Vinodkumar, Hain, C., Peters-Lidard, C., Mahanama, S.P., Arsenault, K.R., Nie, W., Getirana, A., 2020. The 2019–2020 Australian drought and bushfires altered the partitioning of hydrological fluxes. *Geophys. Res. Lett.*, e2020GL091411.
- Matthews, S., 2013. Dead fuel moisture research: 1991–2012. *Int. J. Wildland Fire* 23, 78–92. <https://doi.org/10.1071/WF13005>.
- Nelson, R.M., 2001. Water relations of forest fuels. In: Johnson, E.A., Miyanishi, K. (Eds.), *Forest fires: Behavior and ecological effects*. Academic Press, San Diego, California, pp. 79–149.
- Pellizzaro, G., Cesaraccio, C., Duce, P., Ventura, A., Zara, P., 2007. Relationships between seasonal patterns of live fuel moisture and meteorological drought indices for Mediterranean shrubland species. *Int. J. Wildland Fire* 16 (2), 232–241.
- Puri, K., Dietachmayer, G., Steinle, P., Dix, M., Rikus, L., Logan, L., ..., Bermous, I., 2013. Implementation of the initial ACCESS numerical weather prediction system. *Aust. Meteorol. Oceanogr. J.* 63, 265–284.
- Rigden, A.J., Powell, R.S., Trevino, A., McColl, K.A., Huybers, P., 2020. Microwave Retrievals of Soil Moisture Improve Grassland Wildfire Predictions. *Geophys. Res. Lett.* 47, e2020GL091410 <https://doi.org/10.1029/2020GL091410>.
- Sharma, S., Carlson, J.D., Krueger, E.S., Engle, D.M., Twidwell, D., Fuhlendorf, S.D., Patrignani, A., Feng, L., Ochsner, T.E., 2020. Soil moisture as an indicator of growing-season herbaceous fuel moisture and curing rate in grasslands. *Int. J. Wildland Fire*. <https://doi.org/10.1071/WF19193>.
- Strahler, A.H., and Muller, J.P., 1999: MODIS BRDF Albedo Product: algorithm Theoretical Basis Document Version 5.0., pp. 53.
- Viegas, D.X., Piñol, J., Viegas, M.T., Ogaya, R., 2001. Estimating live fine fuels moisture content using meteorologically based indices. *Int. J. Wildland Fire* 10, 223–240.
- Viney, N.R., 1991. A Review of Fine Fuel Moisture Modelling. *Int. J. Wildland Fire* 1, 215–234. <https://doi.org/10.1071/WF9910215>.
- Vinodkumar, Dharssi, I., 2019. Evaluation and calibration of a high-resolution soil moisture product for wildfire prediction and management. *Agric. For. Meteorol.* 264, 27–39.
- Vinodkumar, Dharssi, I., Bally, J., Steinle, P., McJanet, D., Walker, J., 2017. Comparison of soil wetness from multiple models over Australia with observations. *Water Resour. Res.* 633–646.
- Williams, K., Clark, D., 2014. Disaggregation of daily data in JULES, Hadley Centre technical note 96. Hadley Centre, Met Office, UK.
- Wilson, S.D., 1993. Belowground competition in forest and prairie. *Oikos* 146–150.
- Yang, Y., Donohue, R.J., McVicar, T.R., 2016. Global estimation of effective plant rooting depth: Implications for hydrological modeling. *Water Resour. Res.* 52 (10), 8260–8276.
- Yebra, M., Quan, X., Riaño, D., Larraondo, P.R., van Dijk, A.I., Cary, G.J., 2018. A fuel moisture content and flammability monitoring methodology for continental Australia based on optical remote sensing. *Remote Sens. Environ.* 212, 260–272.
- Yebra, M., Scorteccini, G., Badi, A., Beget, M.E., Boer, M.M., Bradstock, R., Chuvieco, E., Danson, F.M., Dennison, P., Resco de Dios, V., Di Bella, C.M., Forsyth, G., Frost, P., Garcia, M., Hamdi, A., He, B., Jolly, M., Kraaij, T., Martín, M.P., Mouillot, F., Newnham, G., Nolan, R.H., Pellizzaro, G., Qi, Y., Quan, X., Riaño, D., Roberts, D., Sow, M., Ustin, S., 2019. Globe-LFMC, a global plant water status database for vegetation ecophysiology and wildfire applications. *Sci. Data* 6, 155.